Subsurface damages beneath fracture pits of reaction-bonded silicon carbide after ultra-precision grinding

Zhipeng Li[a*], Feihu Zhang[a], Xichun Luo[b]

[a] School of Mechatronics Engineering, Harbin Institute of Technology, Harbin, China

[b] Centre for Precision Manufacturing, DMEM, University of Strathclyde, Glasgow, UK

Corresponding author: Zhipeng Li, E-mail: zplihit@163.com, Telephone: +86 15004680642

Abstract

This paper investigated the structural defects beneath the fracture area of 6H-SiC in reaction-bonded silicon carbide (RB-SiC) ceramics after ultra-precision grinding. The nano-indentation technique was used to evaluate the evolution of deformation behavior and find the critical transition condition among elastic, plastic and fracture. It was found that beneath the fracture pits, dislocations accompanied with micro-cracks (lateral and median) were the two types of subsurface damage. However, no amorphous phase was detected. In addition, a two-beam analysis confirmed that the dislocations were activated on basal <a> and dissociated into the Shockley partial dislocations in 6H-SiC particle. The following indentation experiments revealed that the existence dislocations in the ground subsurface should be occurred earlier than cleavage. These dislocations were the predominant yielding mechanism in 6H-SiC, which initiated at a shear stress of about 23.4-28.4 Gpa through a pop-in event on load-displacement curve. Afterwards, cracks emerged when the maximum tensile stress beneath the indenter increased to 31.6

Gpa. It was identified that cracks could be activated under the intersection effect of non-uniform high density dislocations. Meanwhile, the blocking effect on sliding motion of dislocations caused by cross propagating dislocations, phase boundary and sintering agents play an important role in the evolution of fracture during grinding process. At last, the deformation behavior was further elaborated to discuss the slippage on the basal plane determined by Schmidt factor and structure characteristic of 6H-SiC.

Keywords: RB-SiC, basal < a> dislocation, amorphous, sintering agents, brittle fracture

1. Introduction

RB-SiC ceramics is a composite material that comprise of SiC, Si, grain/phase boundary. For decades, it has attracted much attention as a prospective material to be used in high temperature and corrosive environment due to its high thermal conductivity, thermal shock resistance and high chemical inertness [1, 2]. It is also a favorite candidate substrate material for large-scale lightweight mirrors for space-related applications, in which ultra-smooth machined surfaces are required [3, 4]. However, on account of sp^3 orbital hybridization, the tetrahedral covalent bonds of SiC makes it very difficult to machine even utilizing the hardest diamond tool. Any brittle fracture induced damage will dramatically degrade the performance and mechanical strength of the RB-SiC based devices [5]. To solve this problem, transferring brittle to ductile mode removal is required for realizing mirror finish on the machined SiC surfaces. In a simulation study of single-grit diamond grinding of SiC, Zhu et al. [6] found that once maximum undeformed chip thickness exceed 0.3 μm brittle fracture occurred and transverse cracks initiated. Xiao et al. [7] performed molecular dynamic (MD) simulation study of diamond turning of 6H-SiC and proposed that the primary mechanism for the ductile deformation is Frank partial dislocations and basal plane

edge dislocations. Some high pressure phase transformation also appeared in the residual subsurface. On the contrary, Yan et al. [8] concluded that 6H-SiC just underwent dislocations through conducting Raman spectrum analysis on the diamond turned surface of RB-SiC. Zhang et al. [9] identified that pulverization and cracking were the two types of subsurface damages in grinding pressureless sintered SiC. However, another micro grinding of RB-SiC study has proposed that amorphization (High-Pressure Phase Transformation, HPPT) occurred for both SiC and Si phases in the outmost layer according the result of X-ray diffraction (XRD) detection [10].

What's more, in order to simplify the grinding process, nano-scratch and nano-indentation tests using Berkovich indenter were always carried out by researchers. Zhang et al. [11] performed nano-scratch tests on 6H-SiC and found the brittle-ductile transition's critical depth is around 75 nm when the applied normal load is about 12.2 mN. They also built a simulation model to reveal the relationship between the applied normal load and machined depth [12]. However, such results are mostly suitable for specific single crystal and basal plane. In a recent study, a weak anisotropy especially for hardness and elastic modulus of 6H-SiC was testified by Datye et al. using nano-indentation [13]. Therefore, the SiC grain in RB-SiC ceramics subject more complicate state due to uncertain grain orientation and the coexistence of Si phase and grain/phase boundary. Besides, in the nano-indentation of 6H-SiC (0001) Yin et al. [13] found that the no cracks were occurred when the normal loads up to 400mN, which has controversy with the findings in reference [11]. In the aspect of deformation mechanism, Yan et al. [14] found that polycrystalline structure and median cracks occurred in the nano-indentation subsurface of a nitro-doped N-type sinlge-crystal 6H-SiC wafer. While, Meng et al. [15] just found the amorphous structure under the scratch bottom in 6H-SiC.

Thus, it can be concluded that the researches on the ductile to brittle (DB) transition mechanism and formation mechanism of subsurface damage in diamond machining of SiC are inconclusive. There is no report on direct observation of subsurface damage in the grinding induced fracture area of RB-SiC ceramics, although it can help gain understanding of the subsurface micro-defects formation and the DB transition mechanisms.

In this paper, the subsurface damage underneath the brittle fracture area induced by grinding were investigated through transmission electron microscopy (TEM) observation. The original subsurface structure of RB-SiC ceramics were also exhibited, which could help to verify the defects observed underneath the fracture area indeed created by grinding. However, TEM detection results are just the final state of the damage. So it is significant to restore the dynamic evolution of damage for finding the critical condition of DB transition. To realize this, the interaction between diamond grit and workpiece was always simplied as continuous indent process in previous studies [16, 17]. Therefore, the nano-indentation experiments were conducted for the purpose of analyzing the fracture evolution process and explaining the damage mechanism found in subsurface. At last, combining with the Hexagonal close packed (HCP) structure features and the theoretical value of Schimit factor, the dislocations formation mechanism in 6H-SiC grain was discussed. It hopes that this result will allow for an in-depth understanding of the critical condition of DB transition in ultra-precision grinding of RB-SiC and material structure influence on the evolution of brittle fracture.

2. Experiments

2.1 Material preperation

The test specimen of RB-SiC material was offered by Goodfellow Cambridge Ltd.

(UK). The workpiece dimension is 12.5×12.5×5 mm. For indentation trails and identification original structural defects, the RB-SiC specimen was polished with cerium dioxide powders (grit size about 1 μm) until its surface roughness Ra less than 5 nm. The final polished surface topography was shown in **Fig. 1.** From the Energy spectrum results, it can conclude that the dark particles are SiC phase which are embedded in a remaining Si phase.

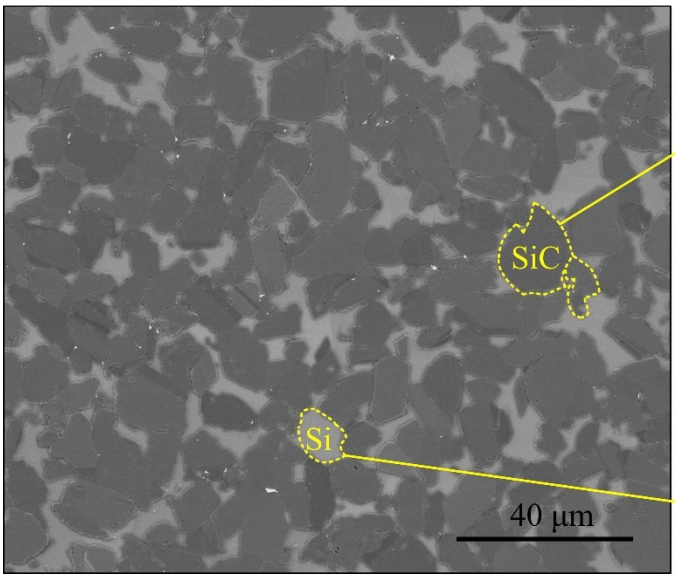

Element	Weight%	Atomic%
C	34.82	55.54
Si	65.18	44.46
Total	100	

Element	Weight%	Atomic%
Si	100	100
Total	100	

Fig. 1. SEM image of surface morphology of the polished specimen and energy spectrum analysis of the corresponding area**.**

2.2 Nano-indentation and grinding experiments

The RB-SiC specimen was ground on a Moore Nanotech 350FG ultra-precision freedom grinder. The detail information of grinding parameters is tabulated in **Table 1**. The machined surface morphology was characterized by a scanning electron microscope (SEM) (Dual beam FEI Helios Nanolab 600i). The cross sectional lamellae for scanning TEM analysis was prepared by focused ion beam (FIB) in-situ etching (Helios Nanolab 600i). The damage morphology beneath polished surface and fracture area of the ground surface were investigated by TEM using a FEI Talos F200x, operated at 300 kV.

After that, the nanoindentation tests were performed using Aligent G200 Nano-indenter fitted with a pyramidal Berkovich indenter at room temperature. The tip radius of Berkovich indenter was measured with AFM as shown in **Fig 2**. The result revealed the tip radius to be about 400 nm. In this context, the blunted geometry of the nanoindenter can be approximated as spherical which is benefit for predicting the elastic response during mechanical contacts using Hertzian law [18]. A series of indentations were conducted on SiC particles at various normal load ranging from 1mN-50mN and each load repeated six times. At the maximum load, a dwell period of 10s was imposed before unloading.

Table 1. Grinding conditions and wheel geometrical parameters

Grinding Parameters	
Diamond wheel	Resin-bonded, 7 µm diamond grit, diameter: 75 mm, width: 6 mm, concentration: 75%.
Truing condition	Green silicon carbon (GC) rod, #800, hardness: P
Coolant	Water-based, challenge 300-HT, concentrations: 2–3%, jet speed:5 m/s, cross-sectional area of nozzle: 12.56 mm^2
Spindle speed	5000 rpm
Feed rate	2 mm/s
Depth of cut	0.5µm, 1.5 µm

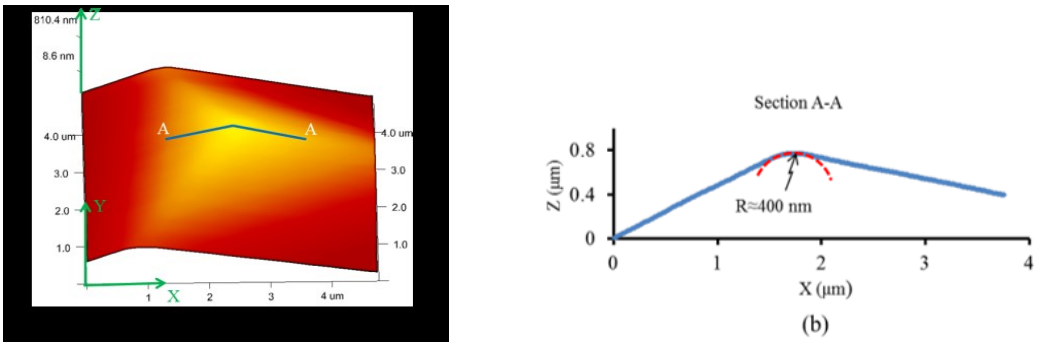

Fig. 2. AFM image of berkovich indenter and the profile of A-A section.

3. Results

3.1 Ground surface morphology

Fig. 3 are the typical SEM micrographs demonstrating the features difference between ductile and semi-ductile ground surfaces of RB-SiC ceramics. As shown in **Fig. 3a**, scratching or ploughing striations are visible on the ground surface. There is no damage can be found, indicating the ductile-regime removal took place while the grinding operated at such smaller cutting depth of 0.5 μm. In contrast, as shown in **Fig. 3b**, the ground surface that was dominated by the combined removal modes of ductile and brittle consists of ploughing grooves and fracture pits areas. From the magnified image **Fig. 3c**, it can be seen that the fracture pits are mainly restricted in the SiC particles. The cleavage fracture with a drape appearance can either be observed and cracks radiated around the fracture pits, both of which are the typical characters of brittle damage for ceramics. Therefore, we can assume that fracture occurred in a transgranular manner.

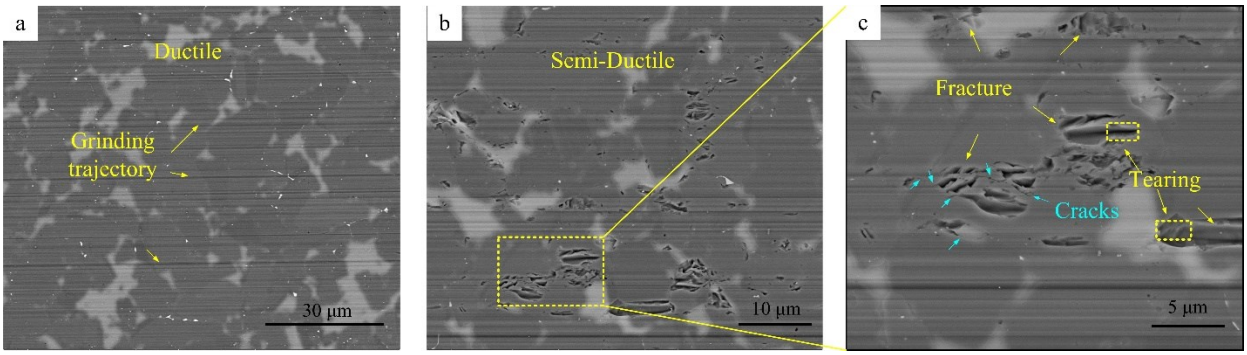

Fig. 3. Ground surface morphology of RB-SiC specimen (a) ductile removal mode (b) semi-ductile removal mode. (c) Enlarge image of the fractured area in image (b).

3.2 Original subsurface structure of RB-SiC

An overview of RB-SiC ceramic structure that underneath the polished surface is shown in **Fig. 4a**. High-Resolution TEM observation and selected area electron diffraction reveals that an amorphous layer formed immediate below polished surface in

Si-I grain. **Fig. 4d** and **e** shows that there are only a few equal thickness fringes produced by residual stress and a high density of stacking faults (SFs) generated by sintering process locating in SiC grains. Moreover, it was found that the structure of the SiC particle was almost dislocation free, thus any subsurface damage must be caused by grinding.

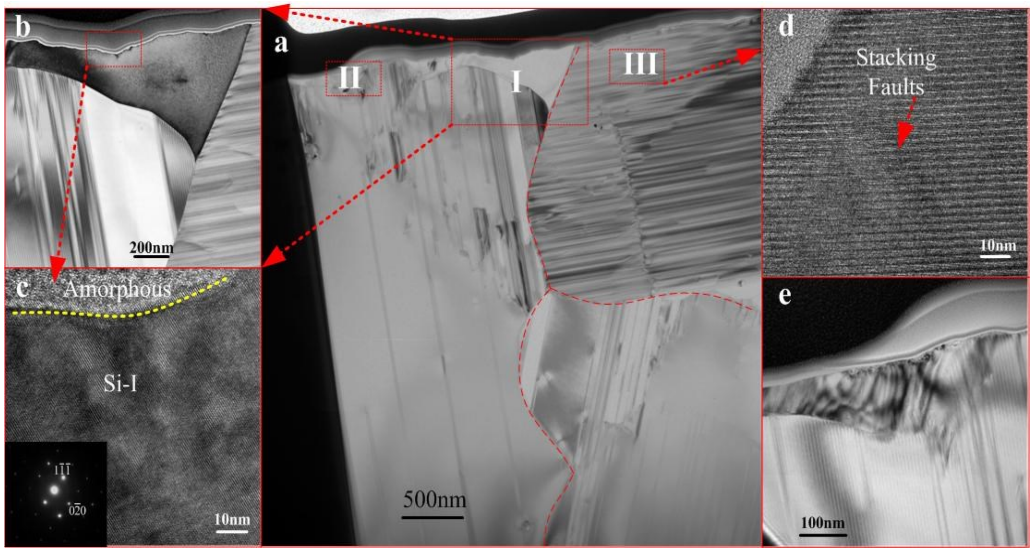

Fig. 4. (a) Cross-sectional Bright field TEM image of the RB-SiC structure after polish, (b) and (e) high magnifications corresponding ‘Ⅰ’ ‘Ⅱ’ zone marked in (a), respectively. (c) and (d) High-Resolution TEM (HRTEM) image of (b) and ‘Ⅲ’ zone in (a).

3.3 Ground induced subsurface defects beneath fracture pits

Fig. 5 presents the cross-sectional TEM image of subsurface damage beneath the ground fracture area of RB-SiC. This zone contain two particles of 6H-SiC. As denoted by arrows in **Fig. 5a**, a high density of non-uniform dislocations accompanying with the lateral crack appeared and approximatly propagated to the depth of 0.52 μm. The crack manifested itself as ‘a coarse band’ due to Moiré fringes [19,20]. In this work, the lateral cracks emanated from the immediate bottom of the surface and fully extended to the adjoining surface of 0.6 μm in width. Further removal of this bulk will result in a

fracture pit as seen on the ground surface (**Fig. 3**). Moreover, it is noteworthy that outside the above region has very localized deformation. No obvious slip band was found, which was different from previous study that slip bands always located aroud cracks. It means the fracture within the SiC particle in RB-SiC ceracmis occurred before macroscopic sliding.

Fig. 5b shows two typical cracks. One was the lateral crack that nulceated from the crystal boundary and terminated within the SiC grain (as marked by arrows). Second was the median crack that started from the groud surface. Likewise, high density dislocations distributed around the cracks. It is apparent that the crack path was microscopically deflected over about 70℃ from the initial direction. Such reorientation might be related to the interaction with the emitted defects (e.g., dislocations [21]) when a crack approaches the last stage of its propagation, it may deviate away from the initial direction, suggesting the complexity of crack propagation [19].

Unfortunately, the grain orientation not strictly satisfy the Bragg condition, the High-Resolution TEM observation of cracks or dislocations was unsuccessful. Therefore, the preparation of another TEM sample was needed to investigate the Burgers vector of these dislocations.

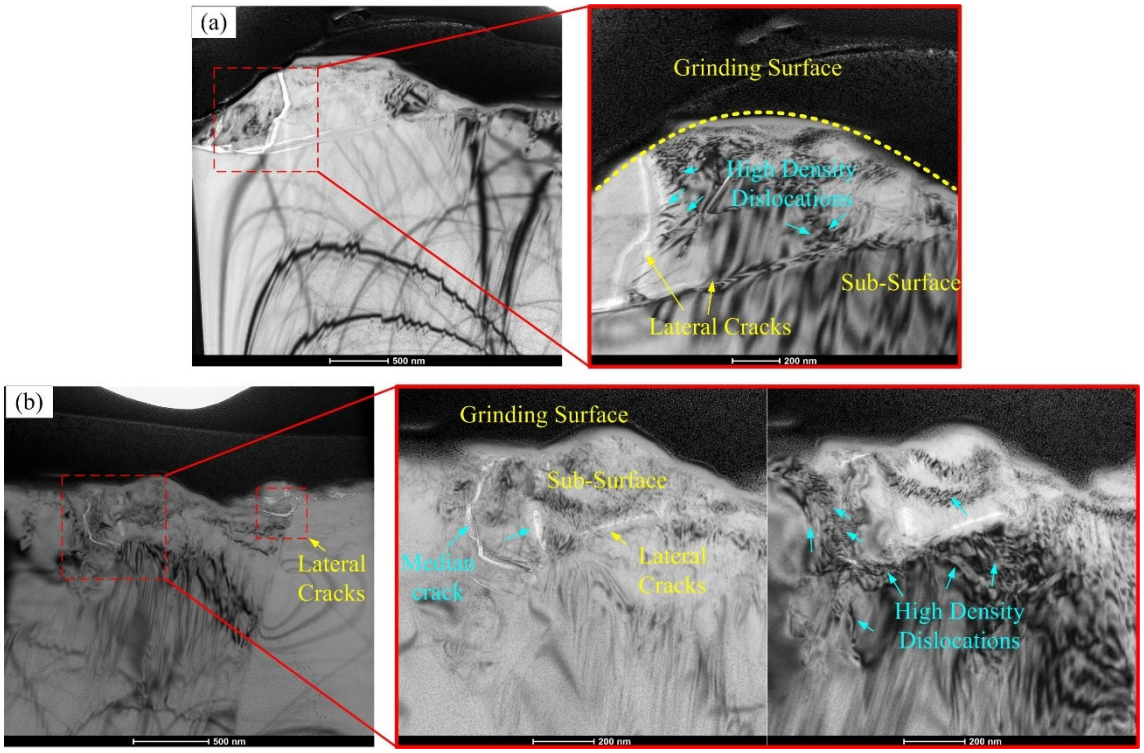

Fig. 5. The typical TEM image of subsurface damage beneath the fracture area.

Fig. 6a depicts such an example, which contains three particles i.e. two 6H-SiC particles and one diamond cubic Si-I particle. The upper part of grinding-induced deformation zone in 6H-SiC grain also assembled a high density of dislocations. These dislocations were stopped by pile-ups at the nodes or dislocation locks where cross developed dislocations interacted (denoted by arrows). Such places usually serve as stress concentrators [22,23] and therefore are extremely undesirable from the point of view of crack preventation, cracks are often initiated at such place. Nevertheless, no evidence of cracks appears. The fully extension of lateral crack might interpret why no cracks existed under the fracture pits (similar the case in **Fig. 5**).

Under the dashed line, some dislocations emitted from the high energy interface of SiC and Si because the interface atoms were deviated from the equilibrium position. **Fig. 6b** shows that some half dislocation loops distributed along the sides of dislocation wall. Both end points of the half loops were pinned by the residual sintering agents, which

suggests that the activation of dislocations is likely via cyclic growth and reconnection calling Frank-read mechanism. Furthermore, the independent residual sintering agents embedded in 'g1' can also serve as initial sites of dislocations as shown in **Fig. 6c**. Thus, it is reasonable to believe that the place with lattice defects such as phase boundary and impurities always act as the preferable nucleation sites of dislocations.

Whereas, in the vicinity of Si-I grain a ten nanometers thickness of amorphous band (β-tin phase) and one system of dislocation ({111} planes) turned up, as shown in **Fig. 6d** and **e**. The phenomenon is consistent with the trends observed in mono-crystalline silicon plastic deformation under complex loading conditions [24]. The plastic deformation via distortion of the atomic lattice of silicon (amorphous phase transformation) takes place first during loading. With the increase of cutting depth, dislocations will nucleate below the amorphous layer. In this case, the amorphous transformation is still the major deformation mechanism as only one slip system of dislocation cannot afford considerable macroscopic plastic deformation.

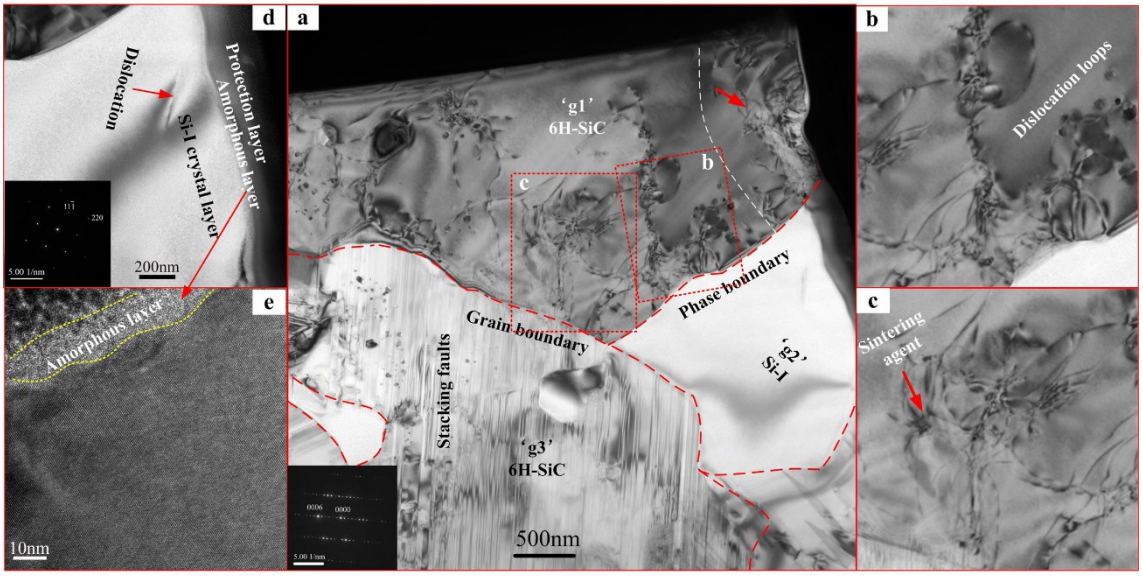

Fig. 6. (a) TEM image of the subsurface structure beneath fracture area; (b to d) high magnifications corresponding ' Ⅰ ' ' Ⅱ ' 'g2' marked in (a), respectively and (e) HRTEM

image of (d).

In order to disclose the structure of dislocations in 6H-SiC particle, a two-beam analysis using invisible criterion $\mathbf{g} \bullet \mathbf{b} = \mathbf{0}$ (**g** is diffraction vector, **b** is Burgers vector) was carried out with different diffraction conditions. **Fig. 7** shows the bright field TEM images under the diffraction vectors of $[\bar{1}100]$, $[11\bar{2}0]$, $[1\bar{2}10]$ and $[0\bar{1}10]$ close to $[0001]$ zone axis. Most of dislocations are out of contrast with diffraction $\boldsymbol{g} = [0\bar{1}10]$, $\boldsymbol{g} = [\bar{1}100]$. Therefore, these dislocations are nearly perfect basal plane dislocations with a Burgers vector $\boldsymbol{b}_1 = \pm(1/3)[\bar{2}110]$ and $\boldsymbol{b}_2 = \pm(1/3)[11\bar{2}0]$. Additionally, though it is difficult to identify individual Burgers vector from the upper part of cluster dislocations, a dislocation reaction is spotted as:

$$[\bar{2}110] \rightarrow [\bar{1}010] + [\bar{1}100] \qquad (1)$$

The **a** and **b** short segments are out of contrast with the diffraction vectors $\boldsymbol{g} = [11\bar{2}0]$ (**Fig. 7b**) and $\boldsymbol{g} = [1\bar{2}10]$ (**Fig. 7c**), which yields to Shockley partial dislocation with Burgers vector $\boldsymbol{b}_a = \pm(1/3)[1\bar{1}00]$ and $\boldsymbol{b}_b = \pm(1/3)[\bar{1}010]$.

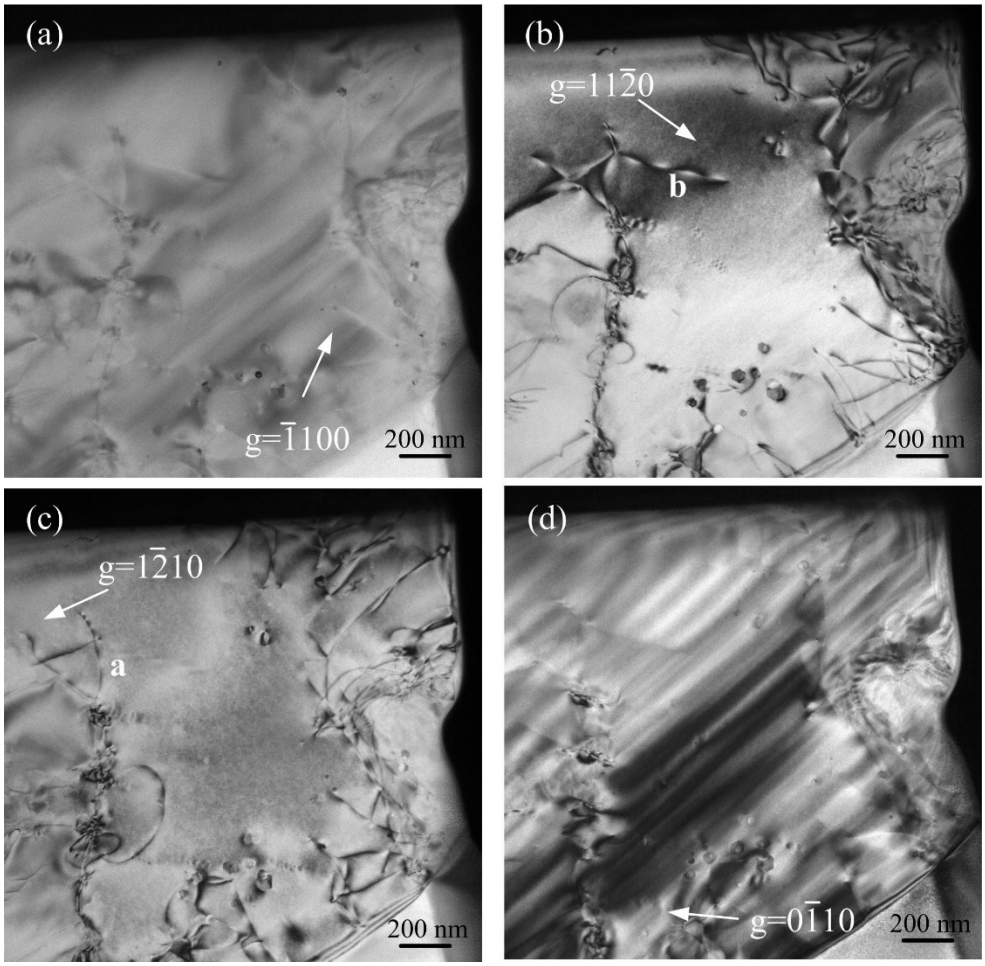

Fig. 7. TEM BF images in two-beam conditions of dislocation underneath 6H-SiC particle (a) $\boldsymbol{g}=[\bar{1}100]$, (b) $\boldsymbol{g}=[11\bar{2}0]$, (c) $\boldsymbol{g}=[1\bar{2}10]$ and (d) $\boldsymbol{g}=[0\bar{1}10]$.

4. Discussion

4.1 Deformation process during nano-indentation

The nano-indentation tests were carried out to find the critical condition between elastic, plastic and brittle fracture deformation presenting beneath the subsurface in 6H-SiC after grinding. **Fig. 8** shows the results of load-displacement (P-h) curves for different peak loads on SiC grain. The P-h response for 1 mN displays an elastic feature. No depth hysteresis are observed in repeat plots. Unlike the indents performed at 1 mN, the indents with peak load of 8mN show a depth hysteresis and a number of discrete

bursts of pop-ins arise on the loading curve. It is obvious that the pop-in loads are typically in the range of 3.99-7.13 mN. The variation of pop-in loads owe to the distribution of defects near the contact area or particle heterogeneity caused by different grain orientations.

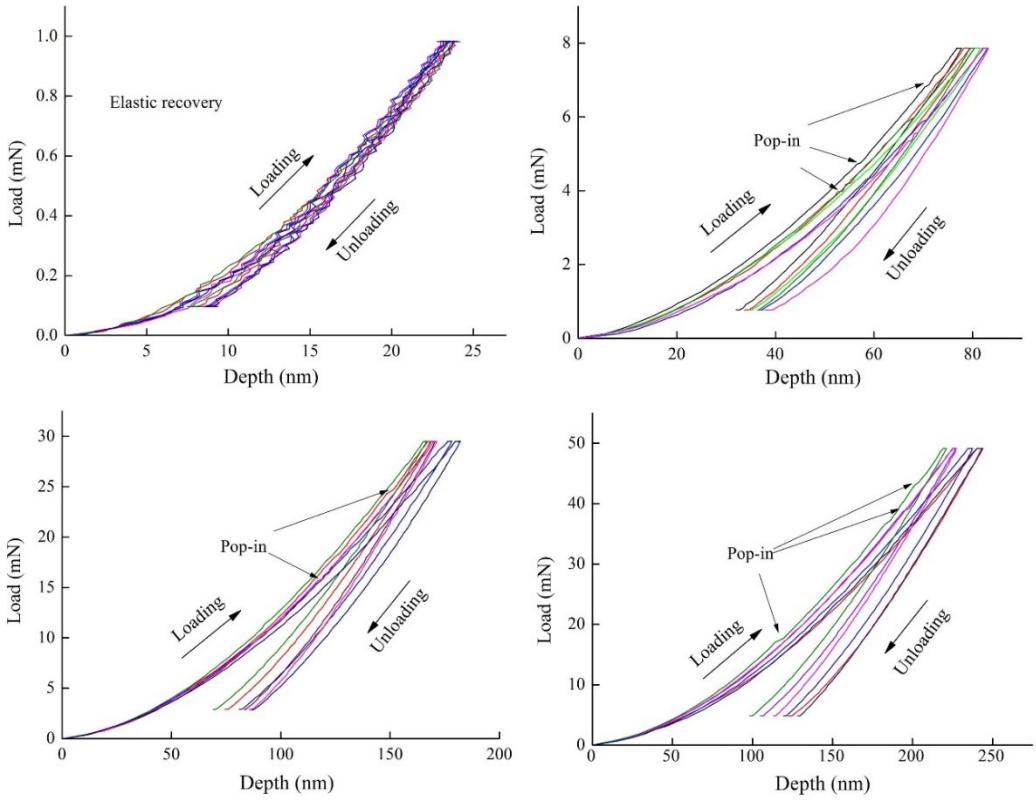

Fig. 8. Load-displacement curves for 6H-SiC grains in RB-SiC ceramics under Berkovich indenter with different normal load.

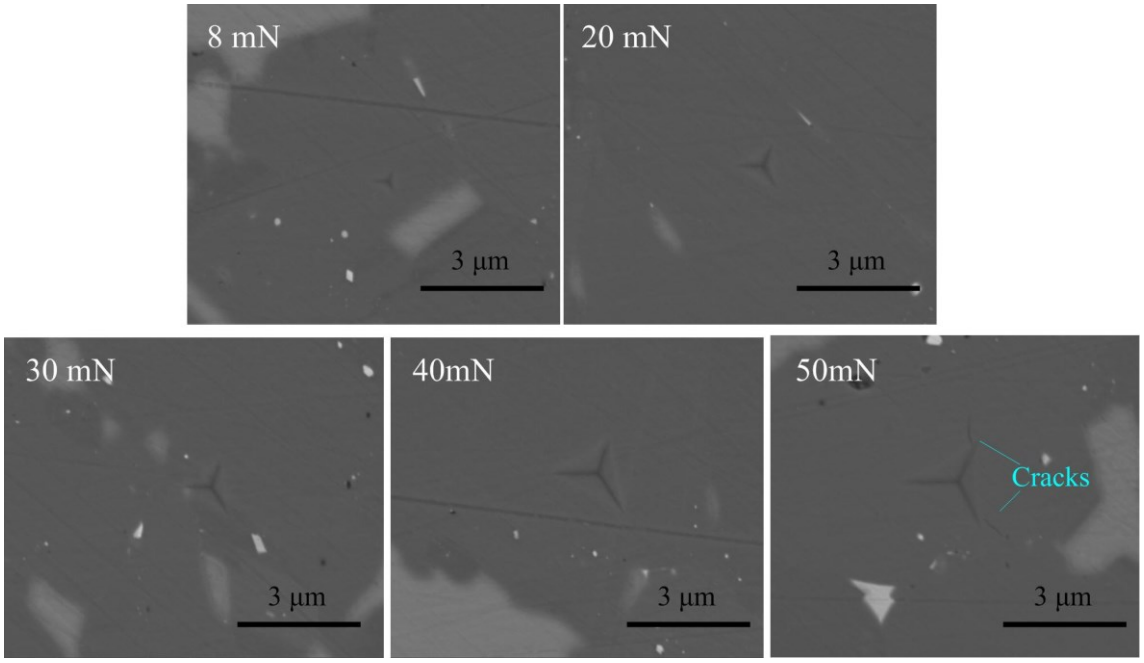

Fig. 9. Representative SEM images showing different damage during Berkovich indentation at different peak loads.

For the material like 6H-SiC, the appearance of bursts implies the nucleation of defects underneath the indentation, which probably attributes to dislocations or micro-cracks. To determine what kind of defects the first pop-in event is related, the shear stress and tensile stress beneath the indenter were calculated according to Hertzian theory. In a defect free material, an incipient of plasticity occurs once local resolved shear stress exceeds the theoretical shear strength of the material. The tensile stress is responsible for cleavage fracture when its value beyond the theoretical cleavage strength.

The maximum shear stress beneath the indenter can be described by the following equation:

$$\tau_{max} = 0.31\left(\frac{6P}{\pi^3}\right)^{1/3}\left(\frac{E^*}{R}\right)^{2/3} \quad (2)$$

Where P is the load of indentation, R is the indenter tip radius, E^* is the reduced

elastic modulus can be expressed as:

$$\frac{1}{E^*} = \frac{1-\upsilon^2}{E} + \frac{1-\upsilon_i^2}{E_i} \quad (3)$$

Where υ and E are the Poisson's ratio and Young's modulus of the 6H-SiC, and the diamond indenter values of E_i and υ_i use 1141 GPa and 0.07 respectively. By putting values of first pop-in loads obtained in **Fig. 8**, the τ_{max} was calculated to be 23.4-28.4 Gpa. The theoretical shear strength of 6H-SiC estimated by $\tau_{th} \approx G/2\pi = 26.1$ GPa , where G is the shear modulus that equal to $E/4\pi(1+\upsilon) = 164.2$ GPa by using E=390 GPa and υ=0.1875 []. Obviously, the maximum shear stress calculated at the loads where the first pop-in happened was closely to the critical shear strength of 6H-SiC. That is to say, the first pop-in event might be arise from plastic deformation in 6H-SiC. Simultaneous, only the maximum tensile stress beneath the indenter is lower than cleavage strength of 6H-SiC, the relationship of pop-in events and plastic deformation can be confirmed.

The maximum tensile stress and cleavage strength can be determined by

$$\sigma_{max} = \left(\frac{1-2\upsilon}{2\pi}\right)\left(\frac{4E^*}{3R}\right)^{2/3} P^{1/3} \quad (4)$$

$$\sigma_{th} = \frac{1}{2}\sqrt{\frac{E\gamma}{a}} \quad (5)$$

Where γ is the surface energy of the cleaved surfaces, a is the original equilibrium interplanar spacing for the cleaved planes. The first pop-in event value of σ_{max} obtained from above equation is 15.7-19.1 Gpa and σ_{th} yields to 32 GPa. This result convince that elastic-plastic transition occurred earlier than cleavage and the first pop-in phenomenon during loading process was controlled by the nucleation of dislocations not

phase transformation (combine with TEM results in **Fig. 5** and **6**).

Following the stage of plastic deformation, cracks emerged from the corner of indenter running on the surface when the normal load increased to 50mN as evidenced in **Fig. 9**. As a comparison, the indentation under 8-40 mN was also displayed, which did not have any evidence of cracking. Therefore, the critical normal load for DB transition must be in the range of 40-50mN. The maximum tensile stress corresponding to that scope was calculated to be about 33.9-36.5 Gpa based on Eq. (2). This tensile stress beyond theoretical value of cleavage strength, indicating that the formation of crack was primarily governed by brittle fracture of cleavage.

Fig. 10 can demonstrate the deformation in 6H-SiC change with the evolution of the shear stress and tensile stress beneath the indenter. In general, when the shear stress achieve about 23.4-28.4 Gpa, the basal planar dislocation $1/3<11\bar{2}0>$ first formed and dissolved into more stable form i.e. partial dislocations. Similarly to the deformation of Mg, the onset of micro yielding is always associated with the activation of basal <a> slip irrespective of the grain distribution and orientation, while the value of the micro yield stress depends on the texture [25]. But there are only two independent slip systems on the basal planes which cannot fulfill von Mises criterion, additional slip or twin systems needs to be activated for arbitrary plastic deformation. Otherwise, the TEM image shown in **Fig. 10a** reveals that the interaction between the perfect and partial of basal plane <a> dislocations results in the formation of junctions. The confined effect of dislocation junctions on dislocation motion becomes increasingly more important with the increase of strain. It provides intrinsic resistance to the movement of dislocations. Hence, there is no way to accommodate the strain along other directions. On the other hand, the interactions between elastic fields originate from lattice mismatch of residual

sintering agents/SiC particles and stress field offered by the dislocations which will increase critical resolved shear stress τ_c (CRSS) needed to active the slip system. Thus, the critical stress required for the crack activation is presumed to be achieved ahead of the stress required for macroscopic sliding plastic deformation. When the tensile strength increased to be about 33.4-36.5 Gpa, the crack might be activated at the interaction place of high density dislocations or grain boundary. Besides, on account of toughening effect of emitted defects i.e. dislocations around the crack tips, the propagation of crack may be impeded or deviate from the fixed lattice plane.

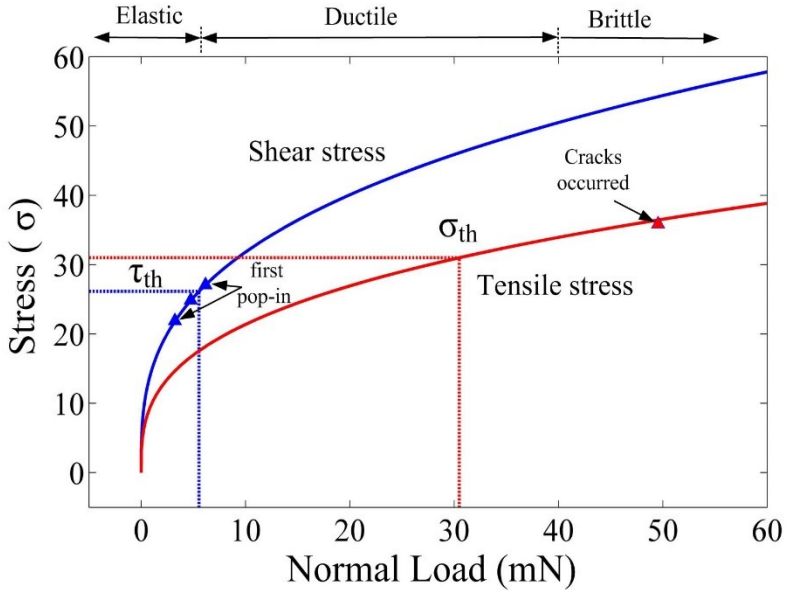

Fig. 10. The calculated shear stress and tensile stress beneath the indenter as their evolution along with the increase of normal load.

3.2 Possible slip system of 6H-SiC in RB-SiC

As shown in **Fig. 11b**, slip system for HCP crystal structure mainly includes $(0001)<11\bar{2}0>$ basal slip, $\{10\bar{1}0\}<11\bar{2}0>$ prismatic slip, $\{10\bar{1}1\}<11\bar{2}0>$ and $\{11\bar{2}2\}<11\bar{2}3>$ pyramidal slip. The activation of dislocation slip is affected by the effective CRSS loading on the slip system, which is given by:

$$\tau_c = \sigma_p \times m_s \tag{6}$$

$$m_s = \cos\varphi \times \cos\lambda \tag{7}$$

Where m_s is the Schmid factor, σ_p is the yield limit, φ and λ are the angles between the loading directions and the slip plane normal and the slip direction, respectively. The CRSS is a comprehensive results including the Pererls-Nabarro stress plus all the possible hardening mechanisms like work-hardening or precipitates. It is independent of the applied stress or crystal orientation. Hence, Schmid factor is related with yield limit and influent the activation of dislocations. The Schmid factor is calculated to analyze the possibility of the activation of particular deformation system in 6H-SiC phase. The loading direction of σ_1, σ_2, σ_3 is assumed to be projected on the basal plane are $0^\circ, 15^\circ, 30^\circ$ as other directions overlap. The angles between the c-axis and the loading directions are defined by θ ranging from 0° to 90° as shown in **Fig. 11a**. The cosine functions of the Schmid factor can be calculated by [26]:

$$\cos\varphi(\lambda) = \frac{\left[u_1u_2 + v_1v_2 - 1/2\,(u_1v_2 + u_2v_1) + (c/a)^2 w_1w_2\right]}{[(u_1^2 + v_1^2 - u_1v_1 + (c/a)^2 w_1^2)(u_2^2 + v_2^2 - u_2v_2 + (c/a)^2 w_2^2)]^{1/2}} \tag{8}$$

Where $[u_1v_1w_1]$ is the 3-index slip plane normal or the slip direction, $[u_2v_2w_2]$ is the loading direction which is the function of θ. c and a are the lattice parameters with the values of 15.117 Å and 3.08065 Å, respectively.

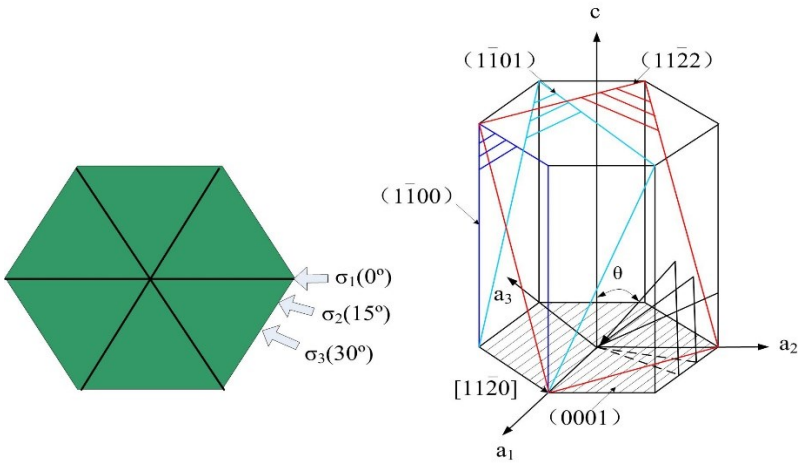

Fig. 11. (a) Loading direction project on basal plane, (b) Slip system in 6H-SiC

The Schmid factor results for the dislocation slip upon loading from three directions ($\sigma_1, \sigma_2, \sigma_3$) are shown in **Fig. 12**. It can be seen that when θ=45° the basal <a> slip possesses the highest m_s (0.5, 0.483 and 0.433). What's more, according to reference [27] the basal dislocation motion is governed by the Peierls mechanism rather than by the solution-hardening mechanism. 6H-SiC densely packed basal {0001} planes along the [1120] directions needs less Pererls-Nabarro stress than other slip system. In addition, available literature suggests that if c/a ratio is greater than 1.633, basal plane is more favorable to slip [28]. The c/a ratio value for 6H-SiC is calculated to 4.907, which is greater than 1.633. Here, greater value of c/a ratio also affirms that the dislocation of SiC are more susceptible to take place on the basal plane slip in comparison to cross slips on $\{10\bar{1}0\}<11\bar{2}0>$ prismatic slip or $\{10\bar{1}1\}<11\bar{2}0>$ and $\{11\bar{2}2\}<11\bar{2}3>$ pyramidal slip.

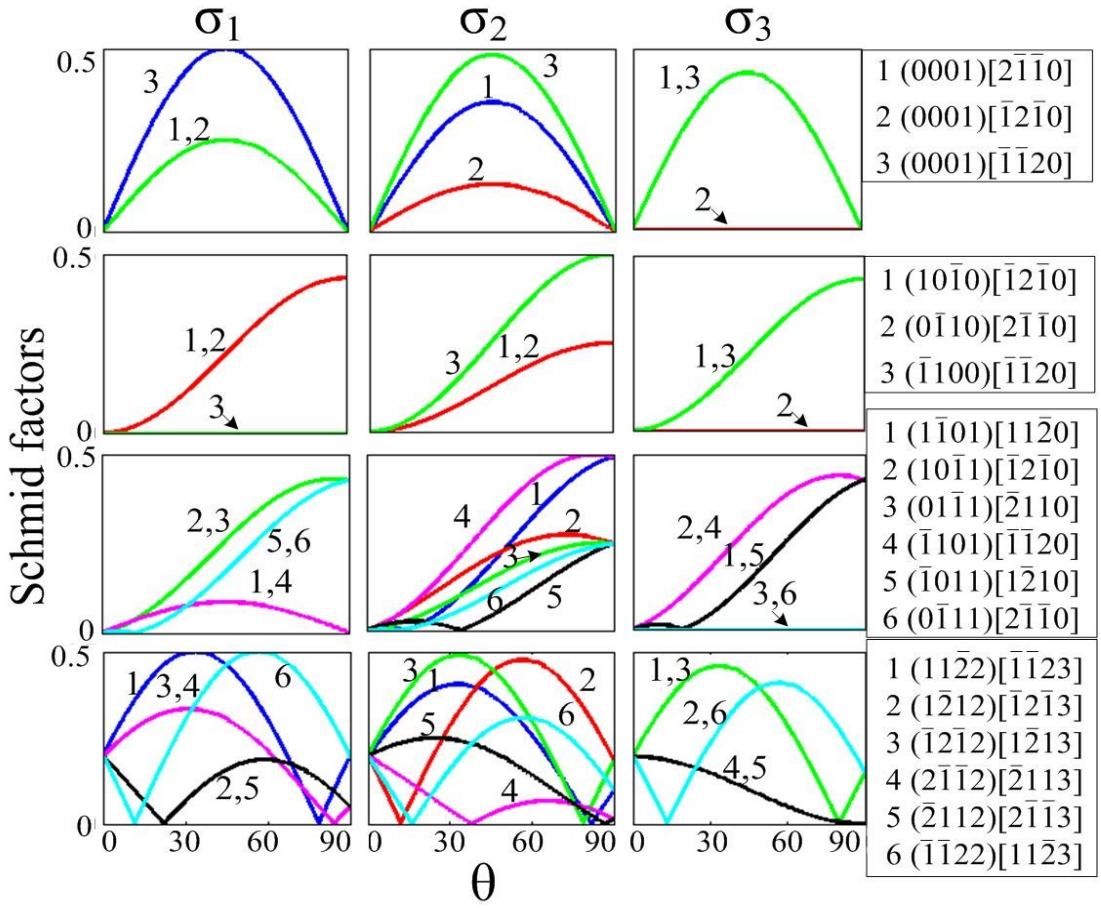

Fig. 12. Schmid factors of (a) basal <a>, (b) prismatic <a>, (c) pyramidal <a>, (d) pyramidal <c+a> slips as a function of the angle between the c-axis and the loading directions<σ_1 σ_2 σ_3>.

Based on aforementioned discussions the fracture deformation process of RB-SiC in ultra-precision grinding are divided into three stages as shown in **Fig 13**. Basal <a> total dislocations, Shockley partial dislocations and dislocation loops are first formed beneath the indenter during loading. The micro-plastic removal mechanism is dominated by basal dislocation nucleation, dissociation and motion. With the increase of load, at the places such as the defects i.e. the phase boundary, the nodes or sintering agents where dislocations pile up, the local tensile stress reaches to maximum cleavage

strength and triggers the formation of micro cracks. Finally, in the process of unloading moment, because the mismatch of elastic and plastic deformation, the lateral crack propagates till to the free surface leading the RB-SiC ceramics removed in brittle fracture mode.

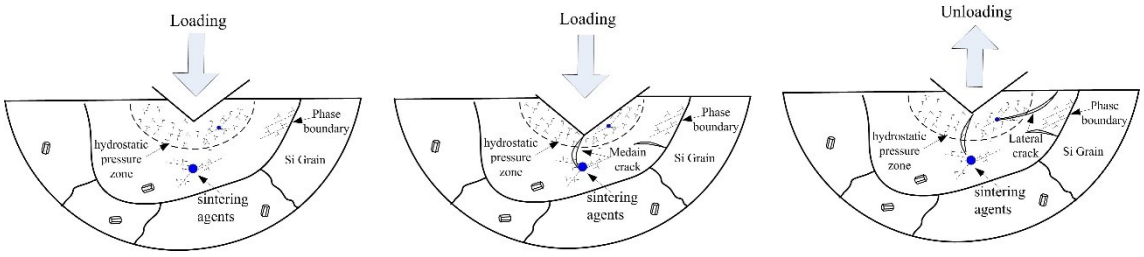

Fig. 13. Schematic of deformation mechanism of 6H-SiC in RB-SiC during ultra-precision grinding process.

5. Conclusion

In this study the structural defects of subsurface beneath the fracture area of RB-SiC ceramics after ultra-precision grinding was explored. The conclusions are summarized as following aspects:

1. Two types of damages were identified beneath the brittle fracture of 6H-SiC particle within the RB-SiC, namely micro cracks and dislocations. The cracks were in the form of lateral and median. The dislocations were including nearly perfect basal-plane dislocations with a Burgers vector of $\boldsymbol{b}=1/3<\bar{2}110>$ and apparent Shockley partial with a Burger vector of $\boldsymbol{b}=1/3[1\bar{1}00]+1/3[\bar{1}010]$. There was no further structural phase transformation found in the subsurface beneath the fracture area. The micro-plastic response of SiC grain is associated with the nucleation, dissociation and motion of dislocations.
2. The residual subsurface defects of silicon grain within the RB-SiC involves in amorphous transformation and {111} plane dislocation. The amorphization of

silicon atoms is the dominant grinding mechanism for plastic deformation which is the same as that in the polishing process.

3. As for nano-indentation of 6H-SiC particle within RB-SiC ceramics using the Berkovich indenter radius 400 nm, the critical shear stress for elastic-plastic transition is about 23.4-28.4 Gpa. The DB transition occurred at the tensile stress of 33.9-36.5 Gpa. In addition, the blocking effect on the sliding motion caused by cross propagating dislocations, phase boundary, and sintering agents play an important role in the evolution of brittle fracture during the grinding process.

Acknowledgements

The authors would like to thank the financial from the National Key Research and Development Program of China (2016YFB1102204) for this study.

References

[1] S. Goel, The current understanding on the diamond machining of silicon carbide, J. Phys. D. Appl. Phys. 47 (2014) 243001.

[2] M. Ishihara, S. Baba, T. Takahashi, T. Arai, K. Hayashi, Fundamental thermo mechanical properties of SiC-based structural ceramics subjected to high energy particle irradiations, Fusion Eng. Des. 51–52 (2000) 117–121.

[3] Robichaud, Joseph L, SiC optics for EUV, UV, and visible space missions, Proceedings of SPIE. 4854 (2003) 39-49.

[4] E. Sein, Y. Toulemont, F. Safa, M. Duran, P. Deny, D. De Chambure, T. Passvogel, G. Pilbratt, A Φ 3.5 M SiC telescope for HERSCHEL mission, IR Sp. Telesc. Instruments. 4850 (2002) 606–618.

[5] K. Li, T. Warren Liao, Surface/subsurface damage and the fracture strength of ground ceramics, J. Mater. Process. Technol. 57 (1996) 207–220.

[6] D. Zhu, S. Yan, B. Li, Single-grit modeling and simulation of crack initiation and propagation in SiC grinding using maximum undeformed chip thickness, Comput. Mater. Sci. 92 (2014) 13–21.

[7] G. Xiao, S. To, G. Zhang, The mechanism of ductile deformation in ductile regime machining of 6H SiC, Comput. Mater. Sci. 98 (2015) 178–188.

[8] J. Yan, Z. Zhang, T. Kuriyagawa, Mechanism for material removal in diamond turning of reaction-bonded silicon carbide, Int. J. Mach. Tools Manuf. 49 (2009) 366–374.

[9] B. Zhang, X.L. Zheng, H. Tokura, M. Yoshikawa, Grinding induced damage in ceramics, J. Mater. Process. Technol. 132 (2003) 353–364.

[10] Q. Zhang, S. To, Q. Zhao, B. Guo, Amorphization and C segregation based surface generation of Reaction-Bonded SiC/Si composites under micro-grinding, Int. J. Mach. Tools Manuf. 95 (2015) 78–81.

[11] B. Meng, F. Zhang, Z. Li, Deformation and removal characteristics in nanoscratching of 6H-SiC with Berkovich indenter, Mater. Sci. Semicond. Process. 31 (2015) 160–165.

[12] F. Zhang, B. Meng, Y. Geng, Y. Zhang, Applied Surface Science Study on the machined depth when nanoscratching on 6H-SiC using Berkovich indenter : Modelling and experimental study, Appl. Surf. Sci. 368 (2016) 449–455.

[13] L. Yin, E.Y.J. Vancoille, K. Ramesh, H. Huang, Surface characterization of 6H-SiC (0001) substrates in indentation and abrasive machining, Int. J. Mach. Tools Manuf. 44 (2004) 607–615.

[14] J. Yan, X. Gai, H. Harada, Subsurface Damage of Single Crystalline Silicon Carbide in Nanoindentation Tests, 10 (2010).

[15] B. Meng, Y. Zhang, F. Zhang, Material removal mechanism of 6H-SiC studied by nano-scratching with Berkovich indenter, Appl. Phys. A. 122 (2016) 1–9.

[16] I. Inasaki, Grinding of Hard and Brittle Materials, CIRP Ann. - Manuf. Technol. 36 (1987) 463–471.

[17] S. Malkin, J.E. Ritter, Grinding Mechanisms and Strength Degradation for Ceramics, J. Eng. Ind. 111 (1989) 167.

[18] S. Goel, J. Yan, X. Luo, A. Agrawal, Incipient plasticity in 4H-SiC during, J. Mech. Behav. Biomed. Mater. 34 (2014) 330–337.

[19] F. Tang, L. Zhang, Subsurface nanocracking in monocrystalline Si (001) induced by nanoscratching, Eng. Fract. Mech. 124–125 (2014) 262–271.

[20] Amand George, M. Gérard, Dislocation loops at crack tips: nucleation and growth—an experimental study in silicon, Mater. Sci. Eng. A. 164 (1993) 118–134.

[21] Hirsch PB, Roberts SG. The brittle-ductile transition in silicon, Philos Mag A. 64 (1991) 55-80.

[22] I. Zarudi, L. Zhang, Subsurface damage in single-crystal silicon due to grinding and polishing, J. Mater. Sci. Lett. 15 (1996) 586–587.

[23] B. LAWN in "Fracture of Brittle Solids", edited by E. A. Davis and I. M. Ward, (University Press, Cambridge, 1993) p. 314.

[24] L. Zhang, I. Zarudi, Towards a deeper understanding of plastic deformation in mono-crystalline silicon, Int. J. Mech. Sci. 43 (2001) 1985–1996.

[25] Y.B. Chun, C.H.J. Davies, Texture effect on microyielding of wrought magnesium alloy AZ31, Mater. Sci. Eng. A. 528 (2011) 3489–3495.

[26] X.L. Nan, H.Y. Wang, L. Zhang, J.B. Li, Q.C. Jiang, Calculation of Schmid factors in magnesium: Analysis of deformation behaviors, Scr. Mater. 67 (2012) 443–446.

[27] S. Malkin, T.W. Hwang, Grinding Mechanisms for Ceramics, CIRP Ann. - Manuf. Technol. 45 (1996) 569–580.

[28] R.W. Hertzberg, Deformation and Fracture Mechanics of Engineering Materials, fourth ed., John Wiley&Sons, United States, 1996.